Preparation and Oxygen Permeation of U-Shaped Perovskite Hollow-Fiber Membranes

Yanying Wei, Hongfei Liu, Jian Xue, Zhong Li, and Haihui Wang
School of Chemistry and Chemical Engineering, South China University of Technology, 381 Wushan Road, Guangzhou 510640, China

DOI 10.1002/aic.12321
Published online July 13, 2010 in Wiley Online Library (wileyonlinelibrary.com).

The oxygen permeation of dense U-shaped perovskite hollow-fiber membranes based on $Ba_{0.5}Sr_{0.5}Co_{0.8}Fe_{0.2}O_{3-\delta}$ prepared by a phase inversion spinning process is reported. The perovskite hollow fibers with totally dense wall were obtained with the outer diameter of 1.147 mm and the inner diameter of 0.691 mm. The dependences of the oxygen permeation on the air flow rate on the shell side, the helium flow rate on the core side, the oxygen partial pressures, and the operating temperatures were experimentally investigated. According to the Wagner theory, it follows that the oxygen transport through the U-shaped hollow-fiber membrane is controlled by both surface reaction and bulk diffusion at the temperature ranges of 750–950°C. High oxygen permeation flux of 3.0 ml/(min cm^2) was kept for about 250 h at 950°C under the conditions of the air feed flow rate of 150 ml/min and the helium flow rate of 50 ml/min. © 2010 American Institute of Chemical Engineers *AIChE J,* 57: 975–984, 2011
Keywords: hollow-fiber membrane, oxygen permeation, perovskite, BSCF

Introduction

In recent years, mixed conducting ceramic oxides with oxygen ionic and electronic conductivity have attracted increasing attentions due to their potential applications in the oxygen separation from air,[1,2] in the partial oxidation of methane to syngas,[3–7] in the selective oxidation of hydrocarbons,[8–10] as the cathode of solid oxide fuel cell,[11–13] and for power plants with carbon sequestration.[14,15] For practical applications, a dense oxygen-selective membrane has to show high chemical stability under hard atmospheres and considerable high oxygen permeability under operation conditions as well as the necessary strength to withstand the mechanical stress in the membrane reactor. Furthermore, the material and the membrane should be cheap enough for large-scale industrial applications. To fulfil these requirements, extensive R&D works on the material developments have been performed since Teraoka et al. [16] published their first paper on the oxygen permeability through $La_{1-x}A_xCo_{1-y}Fe_yO_{3-\delta}$ (A referring to alkaline-earth metals). At the same time, different membrane geometries such as disks, tubes, monoliths, capillaries, and hollow fibers as full or graded materials have been developed. So far, mainly disk-shaped membranes with a limited membrane area (<5 cm^2) are used because, they can be easily fabricated by a conventional pressing method. However, this membrane geometry does not meet the requirements for an industrial application because of the low effective area to volume ratio, high temperature sealing problem, and the difficult assembling to a reactor module.[17] Tubular membranes in the cm-scale are developed to reduce the engineering difficulties, such as the problems associated with the high-temperature sealing.[18] On the other hand, the tubular membranes in the cm-scale still have the disadvantages of low ratio of the surface area to the volume and low oxygen permeation flux due to their relatively thick wall, which makes them unfavorable in practice. Recently, increasing activities can be observed in the preparation of oxygen ion conducting membranes in hollow-fiber geometry. Examples are the pioneering papers from the groups of Li,[19–24] Liu,[25–27] and Schiestel,[28–30] as well as the papers by Trunec[31] and Luyten et al.[32] showing that the

Correspondence concerning this article should be addressed to H. Wang at hhwang@scut.edu.cn.

thin-walled ceramic hollow-fiber membrane can be prepared by wet spinning. The hollow fiber is recommended as potential and promising configuration in future industrial applications because, such hollow-fiber membranes possess several advantages, such as a large membrane area per unit volume for oxygen permeation and high oxygen permeation flux due to thin walls as well as easy assembly for large-scale module fabrications.

So far, large research efforts are recently being focused on the linear hollow fibers because of their high packing density of separation area per volume. However, the linear hollow-fiber membrane has the sealing problem at varying temperatures. When both ends of the linear hollow fiber are tightly fixed on the outer host tube at room temperature, the linear hollow fiber will be broken due to the expansion during increasing temperatures. Therefore, a soft connector was recommended to avoid the expansion of hollow fiber during elevating temperature. For example, Liu et al.[33] used a silicon rubber tube to connect hollow fibers and glass tubes by an organic bond. Thursfield and Metcalfe[34] also used a silicone tube for sealing the linear hollow-fiber membranes. Wang et al.[35] sealed an Au-coated hollow fiber with a silicon rubber ring for the high-purity oxygen production by perovskite hollow-fiber membranes swept with steam. Silicone sealant was also used by Tan et al.[36] for the oxygen production through $La_{0.6}Sr_{0.4}Co_{0.2}Fe_{0.8}O_{3-\delta}$ perovskite hollow-fiber membranes. Although the soft connectors like rubber tube or silicon ring helps to make linear hollow fiber gastight at varying temperatures for oxygen permeation testing in laboratories, they cannot tolerate high temperatures and high pressures, which make them unpracticed in the industrial applications.

Herein, we proposed a U-shaped hollow-fiber configuration to solve the problem mentioned above. In the permeation module, two ends of hollow fiber can be fixed on the same side by ceramic sealant, and the hollow fiber can expand and shrink freely during increasing and decreasing temperature. Therefore, in principle, such U-shaped hollow-fiber membrane can solve the sealing problem and avoid the breakage of the membrane due to the expansion or shrinkage at varying temperatures. In this work, the U-shaped hollow-fiber membranes based on the perovskite-type $Ba_{0.5}Sr_{0.5}Co_{0.8}Fe_{0.2}O_{3-\delta}$ (BSCF), which exhibits a high oxygen permeation and good stability,[37] were prepared. The oxygen permeation, the oxygen transport mechanism, and the stability of the U-shaped BSCF hollow-fiber membrane were investigated in detail.

Experimental

The BSCF oxide powder was synthesized by a combined ethylenediaminetetraacetic acid–citrate complexation, which was described in the previous work.[37] The calcined powder was ball-milled for 24 h and then dried using a spray dryer (BüCHI Mini Spray Dryer, B-290) with a nozzle of 1 μm. The obtained fine powder with the particle size of around 1 μm was used for the preparation of the U-shaped hollow-fiber membrane. The U-shaped BSCF hollow fibers were fabricated using a wet-spinning/sintering method. First, the starting solutions were prepared for spinning the hollow-fiber-membrane precursors. A calculated quantity of polyethersulfone (PESf, A-300, BASF) with the additive polyvinyl pyrrolidone (PVP, K30; Boao Biotech, Shanghai, China) was dissolved in the weighed 1-methyl-2-pyrrolidinone (NMP, Analytical Reagent Grade, purity >99.8%, Kermel Chem, Tianjin, China) solvent in a 250-ml wide-neck bottle. After the polymer solution had formed the weighed amount of BSCF powder was then added gradually, while a stirrer (DJ1C-60, Jieruier, Jiangsu, China) was used at a speed of around 400 rpm to ensure that the powder was dispersed uniformly in the polymer solution. The stirring was carried out continuously for at least 48 h before spinning. After the starting solution was degassed at room temperature for 30 min, it was then transferred to a stainless steel reservoir and was again degassed using a vacuum pump for approximately 30 min to remove air bubbles in the solution. The starting solution was pressurized up to 0.1 bar using nitrogen. A spinneret with an orifice diameter and inner diameter of 1.5 and 1.0 mm, respectively, was used to obtain the hollow-fiber precursors. Deionized water and tap water were used as the internal and external coagulants, respectively. The forming hollow-fiber precursors were immersed in deionized water bath at room temperature to complete the solidification process. The BSCF hollow-fiber precursors were cut into 0.4-m pieces before sintering them in a hanging geometry. After drying in air at room temperature for more than 24 h, the BSCF hollow-fiber precursors were sintered at 1150°C for 10 h under the air flow rate of 20 ml/min to remove the polymer. The operating conditions used in the preparation of the U-shaped BSCF hollow-fiber membranes are summarized in Table 1.

Table 1. Preparation Conditions for the U-Shaped BSCF Hollow-Fiber Membranes

Parameter	Value
Compositions of the starting solution (wt %)	
BSCF powder	59.52
PESf, A-300	7.94
NMP	31.75
PVP, K30	0.79
Spinning temperature (°C)	25
Injection rate of internal coagulant (ml/min)	2
Spinning pressure (bar)	0.1
Air gap (cm)	1.0
Sintering temperature (°C)	1150
Sintering time (h)	10
Air flow rate for sintering (ml/min)	20

The U-shaped BSCF hollow-fiber precursors and the sintered BSCF fibers were examined using a scanning electron microscope (SEM, JEOL JSM-6490LA). Only the dense U-shaped hollow-fiber membranes without defects, which were checked by gastight measurements before assembly, were used for oxygen permeation. The oxygen permeation through the U-shaped BSCF hollow-fiber membranes was conducted in a high-temperature permeation apparatus, as shown in Figure 1. The apparatus consisted of a gas supply system and gas mass flow controllers (MFCs), the U-shaped hollow-fiber membrane reactor module with furnace, and online gas chromatograph (GC). All experiments were performed at a total pressure of 1 atm on both sides of the membrane. The U-shaped BSCF hollow-fiber membrane was sealed in a corundum tube (Φ8 mm × 300 mm) with two channels by a

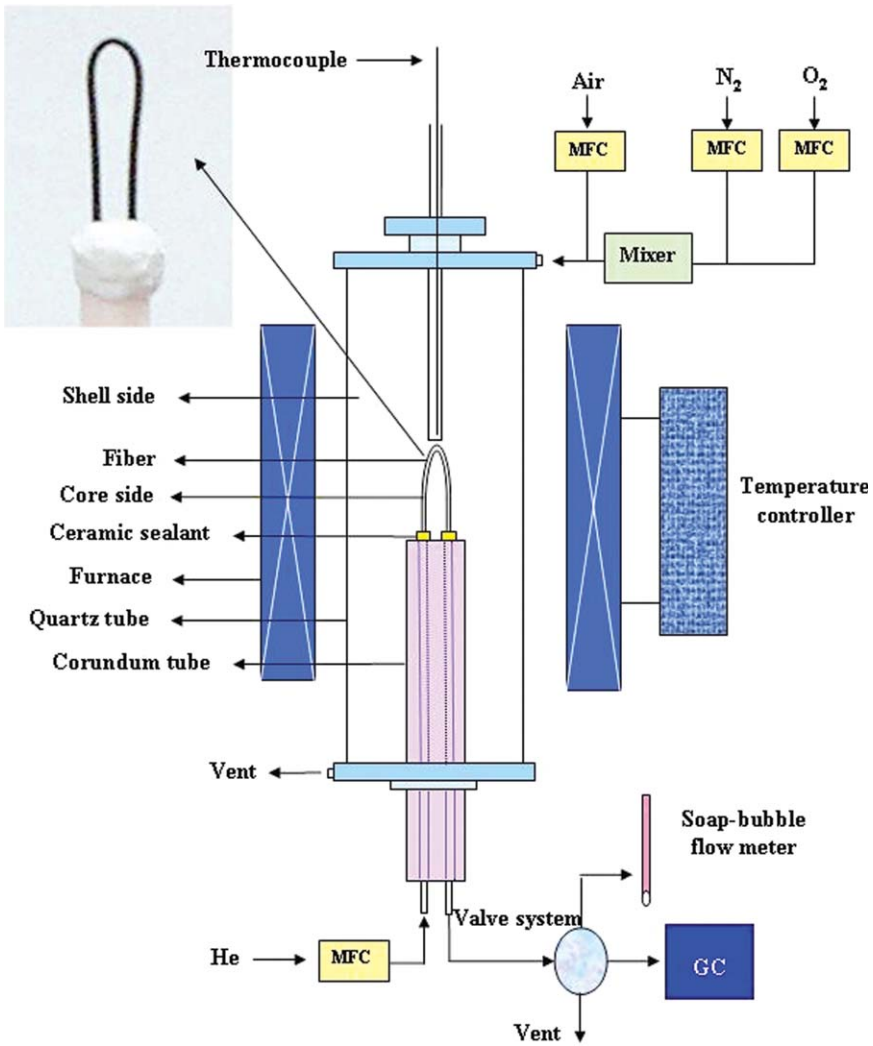

Figure 1. Scheme of the oxygen permeation apparatus for the oxygen permeation of the U-shaped hollow-fiber membrane at high temperature.

[Color figure can be viewed in the online issue, which is available at wileyonlinelibrary.com.]

commercial ceramic sealant (HT767, Huitian, Hubei, China), which was housed in a quartz tube (Φ20 mm × 500 mm). The permeation cell was positioned in a tubular furnace (Φ30 mm × 300 mm), which has an isothermal temperature zone of around 80 mm. Air or a mixture of nitrogen and oxygen was fed to the shell side whereas helium was passed through the core side to collect the permeated oxygen. The flow rate of the gases was controlled by the MFCs (Seven star D08-4F/ZM) calibrated by a soap bubble flow meter. The flow rate of the effluent was also measured by the soap bubble flow meter. The composition of the effluent gas at the exit of the shell side and core side was measured using an online GC (Agilent 7890) with a thermal conductivity detector. The leakage of the oxygen due to the imperfect sealing at high temperatures was less than 0.5% during all the experiments. Assuming that leakage of nitrogen and oxygen through pores or cracks is in accordance with Knudsen diffusion, the fluxes of leaked N_2 and O_2 are related by $J_{N_2}^{Leak}:J_{\sigma_2}^{Leak} = \sqrt{32/28} \times 0.79:0.21 = 4.02$. The O_2 permeation rate was then calculated as follows:

$$J_{O_2}(\mathrm{ml}/(\mathrm{min\ cm}^2)) = \left[C_{O_2} - \frac{C_{N_2}}{4.02}\right]\frac{F}{S} \tag{1}$$

where C_{O_2} and C_{N_2} are the oxygen and nitrogen concentrations calculated from the GC measurements, F the flow rate of the sweep stream, which can be measured by the soap flow meter, and S is the hollow-fiber membrane active area.

Results and Discussion

Figure 2 shows the photos of the U-shaped hollow-fiber precursors and the sintered U-shaped hollow-fiber membrane. After spinning, the hollow-fiber precursors were stored in deionized water bath at room temperature for at least 24 h to remove the residual solvent NMP and complete the solidification process before they were used in the

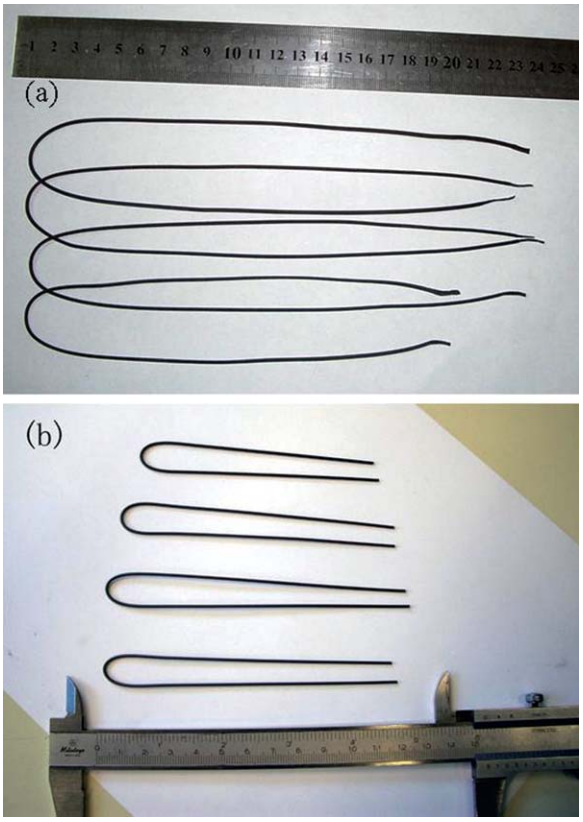

Figure 2. Photos of U-shaped BSCF hollow-fiber membranes.

(a) Hollow-fiber membrane precursor and (b) sintered hollow-fiber membranes. [Color figure can be viewed in the online issue, which is available at wileyonlinelibrary.com.]

sintering process. The BSCF perovskite hollow-fiber precursors obtained were cut into 0.4-m pieces and dried at room temperature in a hanging geometry. During the process of drying in air at room temperature for more than 24 h, the middle part of hollow fiber was suspended on a stick, the two sides of the hollow fiber dropped by gravitation, and then it became U-shaped as shown in Figure 2(a). Then, the U-shaped hollow-fiber precursors were sintered at 1150°C for 10 h under air flow rate of 20 ml/min by hanging in the oven. During sintering, the length and the diameter of the hollow-fiber precursor was reduced from an initial length of 20 cm and an outer diameter of 1.920 mm to a final length of about 14 cm and an outer diameter of about 1.147 mm, as shown in Figure 2(b). The U-shaped configuration can be kept as the precursor one.

Figure 3 presents the SEM pictures of the U-shaped hollow-fiber precursors. It can be seen that finger-like structures have been formed in the fiber precursor, as shown in Figures 3(B) and (C). The outer and inner diameter of the hollow-fiber precursors prepared were 1.920 and 0.973 mm, respectively, as measured from Figure 3A. Figure 3D shows the outer surface of the hollow-fiber precursor, from which it can be seen that the BSCF particles are well dispersed and sparsely connected to each other by the polymer binder. The SEM pictures of the sintered U-shaped BSCF hollow-fiber membrane at 1150°C for 10 h are presented in Figure 4. Compared with the SEM pictures of the hollow-fiber precursors in Figure 3, a significant shrinkage was observed. The outer and inner diameter of the sintered hollow fiber was shrunk to 1.147 and 0.691 mm, respectively. Such a great shrinkage is due to the removal of the polymeric binders and the sintering of the BSCF particles.[38] We can also see from Figures 4(B) and (D) that the finger-like structures, which were observed in the hollow-fiber precursor, disappear and the membrane became totally dense and no open holes can be found in the bulk of the membrane although a large amount of organic additives (about 40 wt %) was used during the spinning process, as shown in Figures 4(E) and (F). Before the U-shaped hollow-fiber membrane was used for the oxygen permeation, the gas tightness was tested at room temperature. No nitrogen was detected on the core side even when the nitrogen partial pressure on the shell side reached 0.5 MPa, which indicated that our hollow-fiber membranes were gastight.

Figure 5 shows the effects of air flow rates on the shell side on the oxygen permeation fluxes through the U-shaped BSCF hollow-fiber membrane at different temperatures. In this experiment, the helium flow rate on the core side was kept at 60 ml/min. When the operating temperature was below 900°C, the oxygen permeation flux increased with the increase of the air flow rate at first, then kept constant after the air flow rate was higher than 100 ml/min. A further increase of the air flow rate did not lead to a further increase of the oxygen permeation flux. In addition, the oxygen flux was more sensitive to the air flow rate at a higher temperature, e.g., 950°C; it was found that the oxygen permeation flux increased with the increase of the air flow rate until it was higher than 150 ml/min. The similar effect of the air flow rate on the oxygen flux at different temperatures has been noted by other researchers.[18,30] Xu et al.[39] investigated the air flow rate dependence on the oxygen permeability through the tubular $La_{0.6}Sr_{0.4}Co_{0.2}Fe_{0.8}O_{3-\delta}$ membrane by modeling. They found that the effect of the change of air flow rate on the oxygen flux was negligible at a large air flow rate because, the change in the air flow rate did not cause apparent changes of the oxygen partial pressure in the upstream. However, a drastic increase in the oxygen permeation flux was predicted at a small air flow rate. Their modeling results also indicated that during the oxygen permeation operation, air should be supplied sufficiently. Our results were also in accordance with their modeling results. To eliminate the effect of the air flow rate on the oxygen permeation flux in a wide range of temperatures, the air flow rate on the shell side was kept constant at 150 ml/min for the following experiments.

Figure 6 presents the oxygen permeation flux through the U-shaped BSCF hollow fiber as a function of helium flow rate at various temperatures. As shown in Figure 6, at the indicated operating temperature the oxygen permeation fluxes through the U-shaped BSCF hollow-fiber membrane increased with the increase of the helium flow rate because, the higher helium flow rate would dilute the permeated oxygen concentration and lower the oxygen partial pressure on the core side. A drastic increase in the oxygen permeation flux was observed when the helium flow rate changed from 20 to 100 ml/min. For example, when the helium flow rate changed from 20 to 100 ml/min, the oxygen partial pressure

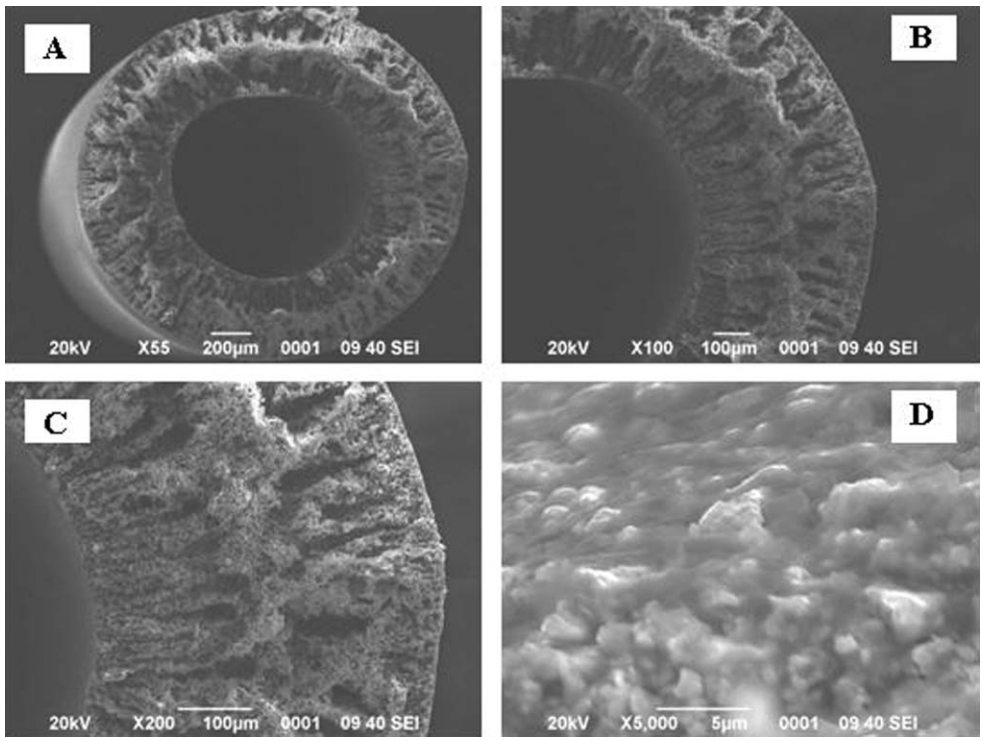

Figure 3. SEM micrographs of the U-shaped BSCF hollow-fiber precursor.

(A) Cross-section; (B) and (C) the wall of the hollow-fiber precursor; and (D) outer surface of the hollow-fiber precursor.

on the core side changed from 0.0792 to 0.0333 bar at 950°C. Therefore, the oxygen permeation fluxes increased drastically with the helium flow rate from 1.75 to 3.49 ml/(min cm^2). For a helium flow rate varying from 100 to 170 ml/min, the oxygen partial pressure on the core side changed from 0.0333 to 0.0228 bar at 950°C, leading to a less obvious change in the oxygen permeation flux. These results are in agreement with the modeling results of Xu.[39] Moreover, Figure 6 also shows that the oxygen permeation fluxes increased with increasing temperatures at the constant helium flow rate because of the enhancement of oxygen ion bulk diffusion and surface reaction rates. For instance, the oxygen permeation flux through the U-shaped hollow-fiber membrane increased from 1.27 to 2.93 ml/(min cm^2) as the temperature was increased from 750 to 950°C at the constant helium flow rate of 60 ml/min. However, the effect of the helium flow rate on the oxygen permeation flux became insensitive at lower temperatures, i.e. below 800°C, because the oxygen partial pressure on the core side varies slightly with the change of the helium flow rate. Similar results were also found by other researchers.[40,41]

Oxygen permeation properties of the U-shaped BSCF hollow-fiber membrane were also studied with different combinations of temperatures and the oxygen partial pressures on the shell side (P_1, atm) and on the core side (P_2, atm). The total flow rate of the oxygen and nitrogen on the shell side was 300 ml/min and different oxygen partial pressures (P_1, atm) on the shell side were obtained by adjusting the ratio of nitrogen and oxygen. The helium flow rate on the core side was kept constant at 100 ml/min. Data were acquired under conditions where P_1 varied step by step while the temperature was kept constant and also under conditions where the temperature varied in steps while P_1 was kept constant. Figure 7 shows the oxygen permeation flux at the temperature range of 700–950°C as a function of the oxygen partial pressures on the shell side. As shown in Figure 7, the oxygen permeation flux increased with the increase of the oxygen partial pressure on the shell side because of the increase of oxygen gradient across the membrane. For instance, the oxygen permeation flux increased from 4.8 to 10.96 ml/(min cm^2) with the increase of the oxygen partial pressure from 0.2 to 1 atm on the shell side. The oxygen permeation flux through the U-shaped hollow-fiber membrane reached 6.93 ml/(min cm^2) under the oxygen partial pressure of 1 atm on the shell side at 875°C, whereas it was even lower than 3.0 ml/(min cm^2) at the same conditions through a tubular BSCF membrane.[18] The temperature dependence of the oxygen permeation flux at various oxygen partial pressures on the shell side is shown in Figure 8. The oxygen permeation flux increased with the increase of temperatures, which can be due to the increase of oxygen diffusion with the increase of temperatures.[18]

For such small wall thickness as found in the U-shaped hollow-fiber geometry, the exchange of oxygen between the oxide surface and the gas phase starts to compete with the oxygen transport through the membrane bulk. To clarify the limiting step of the oxygen permeation through the U-shaped BSCF hollow fiber, the oxygen permeation flux as a function of different oxygen driving forces at various temperatures was investigated, as shown in Figure 9. This dependence can be well described by the Wagner Theory[42–45]:

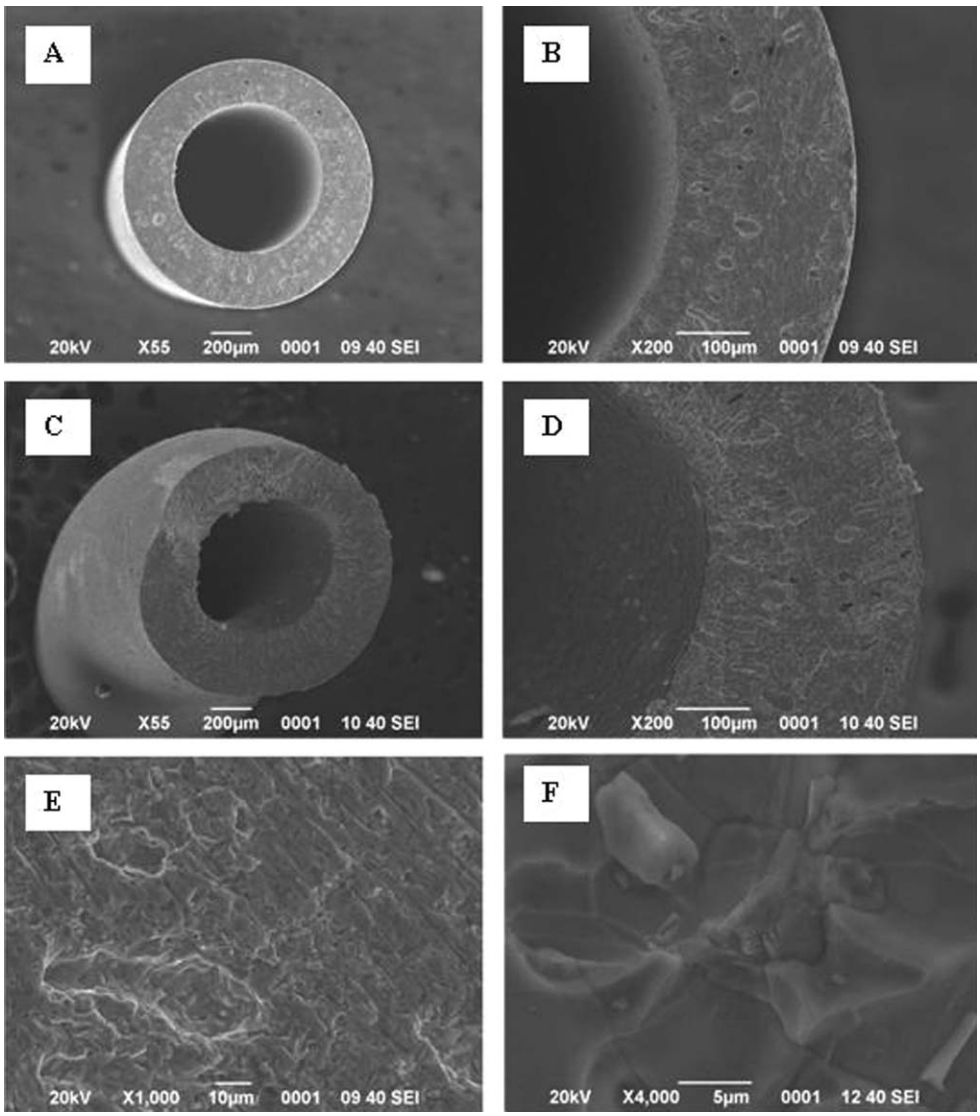

Figure 4. SEM micrographs of the BSCF hollow fibers sintered at 1150°C for 10 h.

(A) Cross-section of sintered fiber; (B) sintered membrane wall; (C) cross-section in the bent region of sintered fiber; (D) sintered membrane wall in the bent region; (E) sintered membrane wall in a high magnification; and (F) outer surface of sintered hollow-fiber membrane.

$$J_{O_2} \approx -\frac{\delta^0 D_v}{4V_m nl}(P_2^n - P_1^n) \quad (2)$$

with δ^0, the number of oxygen defects at $P_0 = 1$ bar; D_v, the vacancy diffusion coefficient ($D_v = D_v^0 e^{E_D/RT}$); E_D, the activation energy of diffusion; V_m, the molar volume of perovskite; l, the wall thickness of membrane; P_1, oxygen partial pressure on the shell side; P_2, oxygen partial pressure on the core side; and n, the fit parameter which can be derived from experimental data of steady-state oxygen permeation.

From the value of n the rate-limiting step of the oxygen permeation can be identified. Generally, for $n < 0$, the bulk diffusion of the oxygen ion is the rate-limiting step, whereas for $n \geq 0.5$, the reaction of the molecular oxygen with the membrane surface is the rate-controlling step. For $0 < n < 0.5$, the oxygen permeation is influenced by both the surface reaction and the bulk diffusion.

A linearized plot of $J_{O_2} \propto (P_2^n - P_1^n)$ with n as a fit parameter is shown in Figure 9. As shown in Figure 9, the n value derived from experimental data decreased from 0.5 to 0.19 as the temperature increased from 700 to 950°C. The experimentally determined coefficient n was 0.5 at 700°C, which indicated that the oxygen permeation flux through the U-shaped BSCF hollow-fiber membrane was controlled by the surface reaction at 700°C. However, the n value derived from the experimental data was between 0.35 and 0.19 at the temperature ranges of 750–950°C, which suggested that the oxygen permeation flux through the U-shaped BSCF hollow-fiber membrane was controlled by both the surface reaction and the bulk diffusion at the temperatures of 750–950°C. In the corresponding Arrhenius plot (shown in Figure

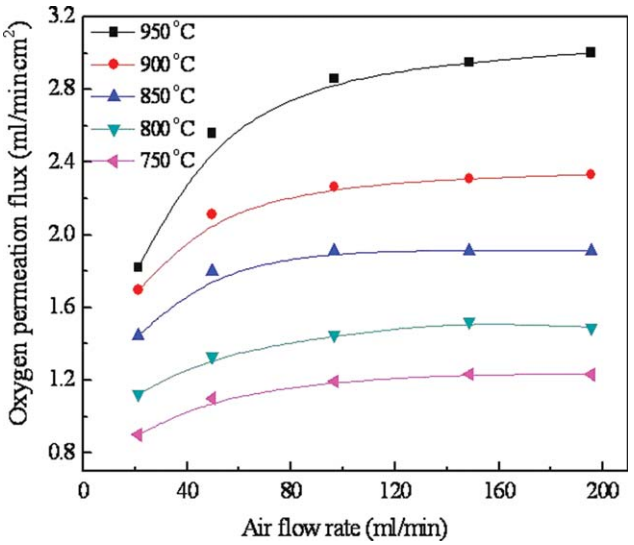

Figure 5. Effects of air feed flow rates on the oxygen permeation flux through the U-shaped BSCF hollow-fiber membrane at different temperatures.

Condition: helium flow rate on the core side was kept at 60 ml/min. [Color figure can be viewed in the online issue, which is available at wileyonlinelibrary.com.]

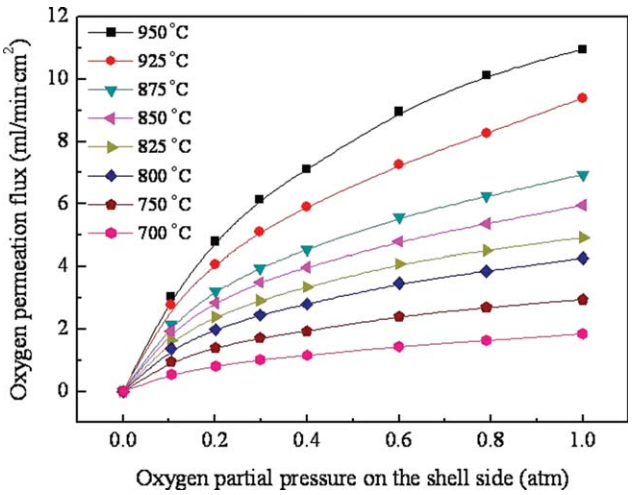

Figure 7. Oxygen permeation fluxes through the U-shaped BSCF hollow-fiber membrane as a function of the oxygen partial pressures on the shell side.

Conditions: the total flow rate of oxygen and nitrogen on the shell side was 300 ml/min and helium flow rate on the core side was 100 ml/min. [Color figure can be viewed in the online issue, which is available at wileyonlinelibrary.com.]

10), a straight line is found which gives an apparent activation energy of 33.2 kJ/mol for the U-shaped hollow-fiber perovskite membrane at the temperature range of 750–950°C.

For practical applications, the oxygen-permeable membrane should not only possess high oxygen permeability, but also have stable oxygen permeation fluxes. Figure 11 shows the time dependence of the oxygen permeation flux through the U-shaped BSCF hollow-fiber membrane at 950°C with air flow rate of 150 ml/min on the shell side and helium flow rate of 50 ml/min on the core side. A steady oxygen permeation flux of 3.0 ml/(min cm^2) was obtained at 950°C during 250 h operation.

Table 2 summarizes the oxygen permeation fluxes through the BSCF membranes in different geometries. As shown in Table 2, the oxygen permeation flux through a BSCF disk membrane with thickness of 1.5 mm was 1.52 ml/(min cm^2)

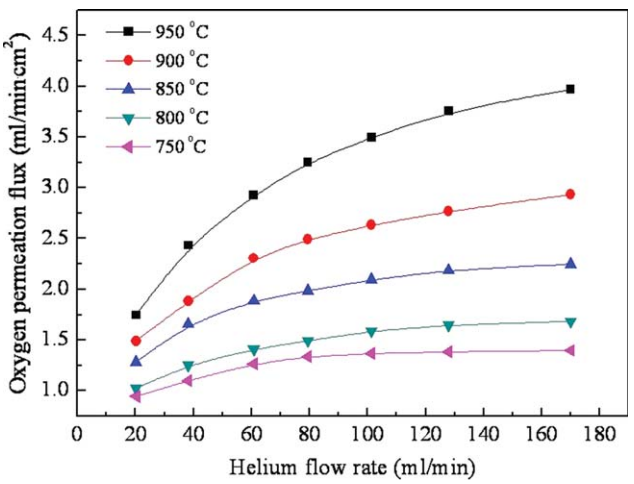

Figure 6. Effects of helium sweep flow rates on the oxygen permeation flux through the U-shaped BSCF hollow-fiber membrane at different temperatures.

Condition: air flow rate on the shell side was kept at 150 ml/min. [Color figure can be viewed in the online issue, which is available at wileyonlinelibrary.com.]

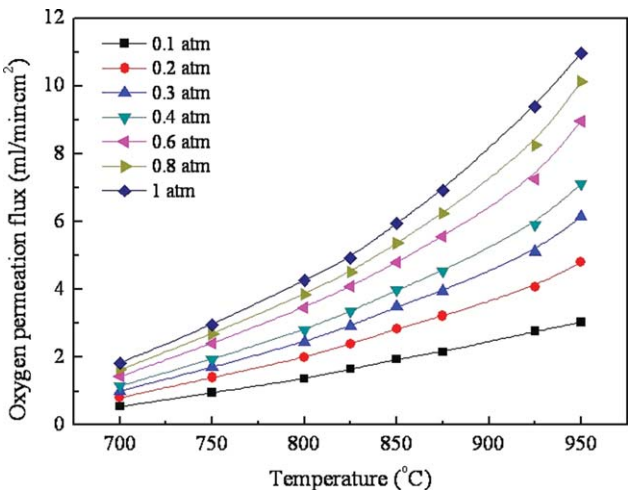

Figure 8. Oxygen permeation fluxes through the U-shaped BSCF hollow-fiber membrane as a function of temperatures.

Conditions: the total flow rate of oxygen and nitrogen on the shell side was 300 ml/min and helium flow rate on the core side was 100 ml/min. [Color figure can be viewed in the online issue, which is available at wileyonlinelibrary.com.]

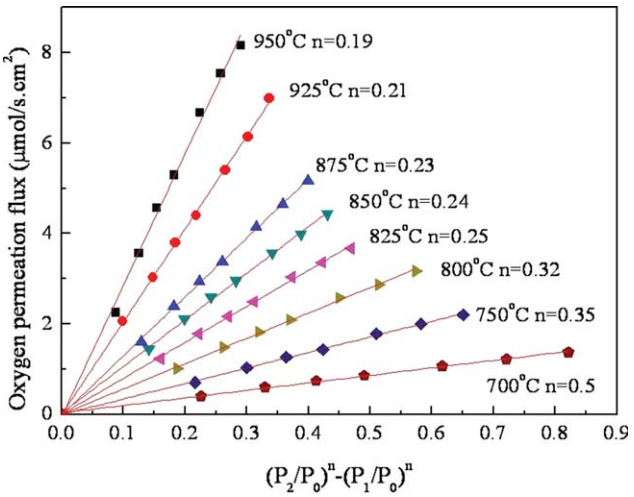

Figure 9. Oxygen permeation fluxes of the U-shaped hollow-fiber membrane against $(P_2/P_0)^n-(P_1/P_0)^n$ at different temperatures.

Conditions: P_1 varied from 0.1 to 1 atm; P_2 varied from 0.0095 to 0.1642 atm; inner diameter of 0.691 mm; outer diameter of 1.147 mm; and membrane area of 1.67 cm^2. [Color figure can be viewed in the online issue, which is available at wileyonlinelibrary.com.]

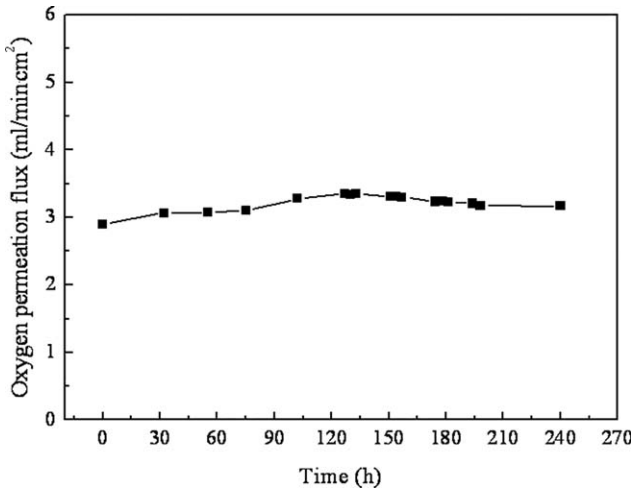

Figure 11. Oxygen permeation flux through the U-shaped BSCF hollow-fiber membrane as a function of time at 950°C.

Conditions: air flow rate on the shell side was 150 ml/min and helium flow rate on the core side was 50 ml/min.

at 950°C with swept helium flow rate of 80 ml/min.[37] A tubular BSCF membrane with the outer and inner diameters of 7.96 and 4.56 mm, respectively was tested by Wang et al.[18] and the oxygen permeation flux was 0.98 ml/(min cm^2) at 850°C with the helium flow rate of 24 ml/min on the core side. Liu et al.[25] found that the oxygen permeation flux through a linear BSCF hollow-fiber membrane was 3.83 ml/(min cm^2) at 950°C with helium flow rate of 80 ml/min. In this study, the oxygen permeation flux through the U-shaped BSCF hollow fiber reached 3.25 ml/(min cm^2) under the same conditions, which is much higher than that of the disk membrane and the tubular membrane while slightly lower than that of the BSCF linear hollow fiber reported by Liu et al.[25] The possible reasons could be the following: the linear BSCF hollow fiber fabricated by Liu et al.[25] had a porous dense asymmetrical microstructure, whereas the U-shaped BSCF hollow fiber in this study was totally dense. Moreover, in this study, the wall of the U-shaped hollow fiber was slightly thicker than that of the linear one reported by Liu and Gavalas.[25]

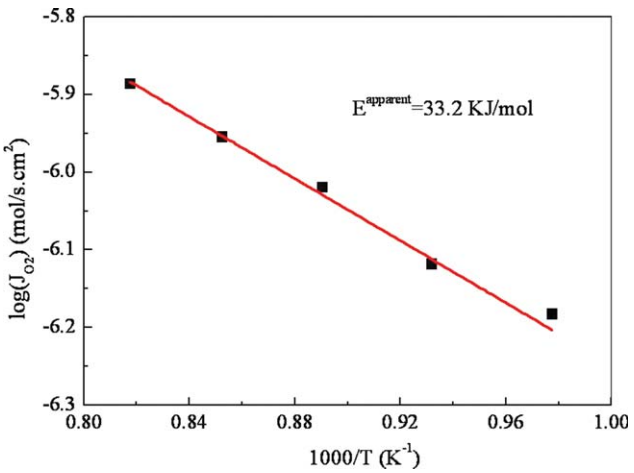

Figure 10. Arrhenius plot of the oxygen permeation flux of the dense U-shaped hollow-fiber perovskite membrane.

Conditions: T = 750–950°C; P_1 = 0.209 bar; and P_2 = 0.059 bar, which was controlled by adjusting the He flow rate. [Color figure can be viewed in the online issue, which is available at wileyonlinelibrary.com.]

Conclusions

The gastight U-shaped BSCF hollow fibers were successfully fabricated for the first time by the phase inversion spinning followed by sintering. The oxygen permeation flux increased with the increase of temperatures and helium flow rates. At first, the oxygen permeation flux increased with the increase of the air flow rate on the shell side, and then became insensitive once the air flow rate reached at an equilibrium value. From the temperature as well as the oxygen concentration gradient dependence of the oxygen permeation flux, it follows that both the surface reaction and the bulk diffusion are the rate-determining steps for the oxygen permeation at the temperature range of 750–950°C, whereas the oxygen permeation is only controlled by the surface reaction at 700°C. A steady oxygen permeation flux of 3.0 ml/(min cm^2) was obtained at 950°C during 250 h operation. These results indicate that the U-shaped BSCF hollow-fiber membrane exhibits good oxygen permeability and stability. Compared with the linear hollow-fiber membrane, the U-shaped hollow-fiber membrane can solve the sealing problem and avoid the breakage of the membrane due to the expansion at varying temperatures in principle, which possibly recommended the U-shaped perovskite hollow fibers suitable for the industrial applications in the future.

Table 2. Comparison of Oxygen Permeation Fluxes Through BSCF Membranes with Different Geometries

Geometries	Character	Conditions	J_{O_2} (ml/(min cm^2))	References
Disk	Thickness = 1.5 mm	A: T = 950°C, helium = 80 ml/min	1.52	37
Tube	O.d. = 7.96 mm, I.d. = 4.56 mm, thickness = 1.7 mm	B: T = 850°C, helium = 24 ml/min	0.98	18
Linear hollow fiber	O.d. = 1.15 mm, I.d. = 0.71 mm, thickness = 0.22 mm	A: T = 950°C, helium = 80 ml/min	3.83	25
		B: T = 850°C, helium = 24 ml/min	1.39	
U-shaped hollow fiber	O.d. = 1.147 mm, I.d. = 0.691 mm, thickness = 0.228 mm	A: T = 950°C, helium = 80 ml/min	3.25	This work
	thickness = 0.228 mm	B: T = 850°C, helium = 24 ml/min	1.37	

Acknowledgments

The authors greatly acknowledge the financial support by National Natural Science Foundation of China (nos. 20706020 and U0834004), the National Basic Research Program of China (no. 2009CB623406), the Science-Technology Plan of Guangzhou City (2009J1-C511-1), and the Fundamental Research Funds for the Central Universities, SCUT (2009220038).

Notation

$J_{N_2}^{Leak}$ = leaked nitrogen flux, ml/(min cm^2)
$J_{O_2}^{Leak}$ = leaked oxygen flux, ml/(min cm^2)
J_{O_2} = oxygen permeation flux, ml/(min cm^2)
C_{O_2} = oxygen concentration, %
C_{N_2} = nitrogen concentration, %
F = total flow rate of the outlet on the sweep side, ml/min
S = membrane area, cm^2
P_1 = oxygen partial pressures on the shell side, bar
P_2 = oxygen partial pressure on the core side, bar
P_0 = standard pressure (P_0 = 1 bar)
D_v = vacancy diffusion coefficient
E_D = activation energy of diffusion
V_m = molar volume of perovskite
R = gas constant (R = 8.3145 J/(mol K))
T = temperature, K
l = thickness of the membrane, mm
n = fit parameter derived from experimental data of steady-state oxygen permeation

Greek letters

δ = number of oxygen defects, $0 < \delta < 1$
δ^0 = number of oxygen defects at P_0

Literature Cited

1. Vente JF, Haije WG, Rak ZS. Performance of functional perovskite membranes for oxygen production. *J Membr Sci*. 2006;276:178–184.
2. Zhu XF, Sun SM, Cong Y, Yang WS. Operation of perovskite membrane under vacuum and elevated pressures for high-purity oxygen production. *J Membr Sci*. 2009;345:47–52.
3. Jiang HQ, Wang HH, Werth S, Schiestel T, Caro J. Simultaneous production of hydrogen and synthesis gas by combining water splitting with partial oxidation of methane in a hollow fiber membrane reactor. *Angew Chem Int Ed*. 2008;47:9341–9344.
4. Gu XH, Jin WQ, Chen CL, Xu NP, Shi J, Ma YH. YSZ–$SrCo_{0.4}Fe_{0.6}O_{3-\delta}$ membranes for the partial oxidation of methane to syngas. *AIChE J*. 2002;48:2051–2060.
5. Chen CS, Feng SJ, Ran S, Zhu DC, Liu W, Bouwmeester HJM. Conversion of methane to syngas by a membrane-based oxidation-reforming process. *Angew Chem Int Ed*. 2003;42:5196–5198.
6. Zhu XF, Wang HH, Cong Y, Yang WS. Partial oxidation of methane to syngas in $BaCe_{0.15}Fe_{0.85}O_{3-d}$ membrane reactors. *Catal Lett*. 2006;111:179–185.
7. Gu XH, Yang L, Tan L, Jin WQ, Zhang LX, Xu NP. Modified operating mode for improving the lifetime of mixed-conducting ceramic membrane reactors in the POM environment. *Ind Eng Chem Res*. 2003;42:795–801.
8. Wang HH, Cong Y, Yang WS. High selectivity of oxidative dehydrogenation of ethane to ethylene in an oxygen permeable membrane reactor. *Chem Commun*. 2002;14:1468–1469.
9. Rebeilleau-Dassonneville M, Rosini S, van Veen AC, Farrusseng D, Mirodatos C. Oxidative activation of ethane on catalytic modified dense ionic oxygen conducting membranes. *Catal Today*. 2005;104:131–137.
10. Akin FT, Lin YS. Selective oxidation of ethane to ethylene in a dense tubular membrane reactor. *J Membr Sci*. 2002;209:457–467.
11. Zhang K, Ge L, Ran R, Shao ZP, Liu SM. Synthesis, characterization and evaluation of cation-ordered $LnBaCo_2O_{5+\delta}$ as materials of oxygen permeation membranes and cathodes of SOFCs. *Acta Mater*. 2008;56:4876–4889.
12. Zeng PY, Ran R, Chen ZH, Zhou W, Gu HX, Shao ZP, Liu SM. Efficient stabilization of cubic perovskite $SrCoO_{3-\delta}$ by B-site low concentration scandium doping combined with sol–gel synthesis. *J Alloys Compd*. 2008;455:465–470.
13. Zheng Y, Ran R, Shao ZP. Cr doping effect in B-site of $La_{0.75}Sr_{0.25}MnO_3$ on its phase stability and performance as an SOFC anode. *Rare Met*. 2009;28:361–366.
14. Ren JY, Fan YQ, Egolfopoulos FN, Tsotsis TT. Membrane-based reactive separations for power generation applications: oxygen lancing. *Chem Eng Sci*. 2003;58:1043–1052.
15. Fan YQ, Ren JY, Onstot W, Pasale J, Tsotsis TT, Egolfopoulos FN. Reactor and technical feasibility aspects of a CO_2 decomposition-based power generation cycle, utilizing a high-temperature membrane reactor. *Ind Eng Chem Res*. 2003;42:2618–2626.
16. Teraoka Y, Zhang HM, Furukawa S, Yamazoe N. Oxygen permeation through perovksite-type oxides. *Chem Lett*. 1985;11:1743–1746.
17. Wang HH, Wang R, Liang DT, Yang WS. Experimental and modeling studies on $Ba_{0.5}Sr_{0.5}Co_{0.8}Fe_{0.2}O_{3-\delta}$ (BSCF) tubular membranes for air separation. *J Membr Sci*. 2004;243:405–415.
18. Wang HH, Cong Y, Yang WS. Oxygen permeation study in a tubular $Ba_{0.5}Sr_{0.5}Co_{0.8}Fe_{0.2}O_{3-\delta}$ oxygen permeation membrane. *J Membr Sci*. 2002;210:259–271.
19. Tan XY, Liu Y, Li K. Mixed conducting ceramic hollow-fiber membranes for air separation. *AIChE J*. 2005;51:1991–2000.
20. Tan XY, Liu YT, Li K. Preparation of LSCF ceramic hollow-fiber membranes for oxygen production by a phase-inversion/sintering technique. *Ind Eng Chem Res*. 2005;44:61–66.
21. Tan XY, Li K. Oxygen production using dense ceramic hollow fiber membrane modules with different operating modes. *AIChE J*. 2007;53:838–845.
22. Tan XY, Liu SM, Li K. Preparation and characterization of inorganic hollow fiber membranes. *J Membr Sci*. 2001;188:87–95.
23. Liu SM, Tan XY, Li K, Hughes R. Preparation and characterisation of $SrCe_{0.95}Yb_{0.05}O_{2.975}$ hollow fiber membranes. *J Membr Sci*. 2001;193:249–260.
24. Liu SM, Li K, Hughes R. Preparation of $SrCe_{0.95}Yb_{0.05}O_{3-\delta}$ perovskite for use as a membrane material in hollow fiber fabrication. *Mater Res Bull*. 2004;39:119–133.
25. Liu SM, Gavalas GR. Oxygen selective ceramic hollow fiber membranes. *J Membr Sci*. 2005;246:103–108.
26. Liu SM, Gavalas GR. Preparation of oxygen ion conducting ceramic hollow-fiber membranes. *Ind Eng Chem Res*. 2005;44:7633–7637.

27. Liu SM, Tan XY, Shao ZP, da Costa JCD. $Ba_{0.5}Sr_{0.5}Co_{0.8}Fe_{0.2}O_{3-\delta}$ ceramic hollow-fiber membranes for oxygen permeation. *AIChE J*. 2006;52:3452–3461.
28. Schiestel T, Kilgus M, Peter S, Caspary KJ, Wang HH, Caro J. Hollow fibre perovskite membranes for oxygen separation. *J Membr Sci*. 2005;258:1–4.
29. Kilgus M, Wang HH, Werth S, Caro J, Schiestel T. Dense perovskite hollow fibre membranes. *Desalination*. 2006;199:355–356.
30. Tablet C, Grubert G, Wang HH, Schiestel T, Schroeder M, Langanke B, Caro J. Oxygen permeation study of perovskite hollow fiber membranes. *Catal Today*. 2005;104:126–130.
31. Trunec M. Fabrication of zirconia- and ceria-based thin-wall tubes by thermoplastic extrusion. *J Eur Ceram Soc*. 2004;24:645–351.
32. Luyten J, Buekenhoudt A, Adriansens W, Cooymans J, Weyten H, Servaes F, Leysen R. Preparation of $LaSrCoFeO_{3-x}$ membranes. *Solid State Ionics*. 2000;135:637–642.
33. Liu H, Pang ZB, Tan XY, Shao Z, Sunarso J, Ding R, Liu SM. Enhanced oxygen permeation through perovskite hollow fiber membranes by methane activation. *Ceram Int*. 2009;35: 1435–1439.
34. Thursfield A, Metcalfe IS. Air separation using a catalytically modified mixed conducting ceramic hollow fiber membrane module. *J Membr Sci*. 2007;288:175–187.
35. Wang HH, Kolsch P, Schiestel T, Tablet C, Werth S, Caro J. Production of high-purity oxygen by perovskite hollow fiber membranes swept with steam. *J Membr Sci*. 2006;284:5–8.
36. Tan XY, Pang ZB, Li K. Oxygen production using $La_{0.6}Sr_{0.4}Co_{0.2}Fe_{0.8}O_{3-\delta}$ (LSCF) perovskite hollow fiber membrane modules. *J Membr Sci*. 2008;310:550–556.
37. Shao ZP, Yang WS, Cong Y, Dong H, Tong JH, Xiong GX. Investigation of the permeation behaviour and stability of a $Ba_{0.5}Sr_{0.5}Co_{0.8}Fe_{0.2}O_{3-\delta}$ oxygen membrane. *J Membr Sci*. 2000; 172:177–188.
38. Wang HH, Schiestel T, Tablet C, Schroeder M, Caro J. Mixed oxygen ion and electron conducting hollow fiber membranes for oxygen separation. *Solid State Ionics*. 2006;177:2255–2259.
39. Xu NP, Li SG, Jin WQ, Shi J, Lin YS. Experimental and modelling study on tubular dense membranes for oxygen permeation. *AIChE J*. 1999;45:2519–2526.
40. Tan XY, Wang ZG, Liu H, Liu SM. Enhancement of oxygen permeation through $La_{0.6}Sr_{0.4}Co_{0.2}Fe_{0.8}O_{3-\delta}$ hollow fiber membranes by surface modifications. *J Membr Sci*. 2008;324:128–135.
41. Meng B, Wang ZG, Tan XY, Liu SM. $SrCo_{0.9}Sc_{0.1}O_{3-\delta}$ perovskite hollow fiber membranes for air separation at intermediate temperatures. *J Eur Ceram Soc*. 2009;29:2815–2822.
42. Wagner C, Schottky W. Beitrag zur Theorie des Anlaufvorganges. *Z Phys Chem B*. 1930;11:25–29.
43. Wagner C. Equations for transport in solid oxides and sulfides of transition metals. *Prog Solid State Chem*. 1975;10:3–16.
44. Akin FT, Lin YS. Oxygen permeation through oxygen ionic or mixed-conducting ceramic membranes with chemical reactions. *J Membr Sci*. 2004;231:133–146.
45. Xu SJ, Thomson WJ. Oxygen permeation rates through ion-conducting perovskite membranes. *Chem Eng Sci*. 1999;54:3839–3850.

Manuscript received Jan. 22, 2010, and revision received Apr. 19, 2010.